

Imaging the Crustal Structure of the Southern Marmara Region (Turkey) Using Aeromagnetic and Gravitational Data

Muhammet Ali Aygün * , Ahmet Sinan Demirel 

Department of Marine Geology and Geophysics, Institute of Marine Sciences and Management, Istanbul University, İstanbul, Türkiye

Corresponding author: M. A. Aygün
E-mail: maygun@ogr.iu.edu.tr

Received 30.11.2024
Accepted 18.12.2024

Abstract

In this study, discontinuities and major tectonic boundaries are interpreted in and around the South Marmara Region through the analysis of airborne Bouguer gravity and magnetic anomalies. Radial average power spectrum (RAPS) and band-pass filtering techniques are employed for the separation of long and short wavelengths. The application of RASP to the entire study area has yielded the detection of four depth segments, which have been employed in conjunction with tilt derivatives for the estimation of structural depth. Furthermore, the radial average depths of these depth segments are 30.5 km, 11.6 km, 3.2 km and 0.52 km. This study aims to gain insight into the crustal characteristics of the South Marmara region through the utilization of geophysical data, with a particular focus on the YDABCAG-198Y231G grid data obtained through the digitization of analogue data from the Aegean region. The relative merits and limitations of general and developed models will be discussed.

Keywords: Airborne Gravity, Airborne Magnetic, Tilt-depth, depth-slicing, South Marmara.

Introduction

Magnetic and gravity data provide valuable insights into the structure and composition of the Earth's lithosphere, aiding in the exploration of its physical and tectonic properties (Milligan and Gunn, 1997). Magnetic data capture variations in the Earth's magnetic field caused by differences in the magnetic susceptibility of subsurface rocks, while gravity data reveal density variations within the crust and upper mantle (Hinze et al, 2013). Together, these methods offer a non-invasive approach to mapping geological structures, such as faults, basins, and magmatic intrusions, and are crucial for understanding lithospheric dynamics (Spector and Grant, 1970). The integration of magnetic and gravity data is particularly useful for delineating crustal thickness, identifying tectonic boundaries, and studying lithospheric deformation processes. These datasets are also essential in resource exploration, helping locate mineral deposits, hydrocarbons, and geothermal reservoirs (Milligan and Gunn, 1997). Additionally, they contribute to assessing geohazards by improving our understanding of fault systems and regional stress fields (Hinze et al, 2013).

Transforming analog gravity and magnetic data into digital formats offers significant advantages that enhance the capabilities of modern geophysical analysis. Analog data, which were previously limited in terms of storage, accessibility, and processing, become far more versatile once digitized. Digital transformation enables the use of advanced computational techniques, allowing for more precise data processing, including filtering, modeling, and inversion to reveal detailed subsurface features. These enhancements are particularly useful in delineating lithospheric structures and locating mineral resources (Blakely, 1995). Additionally, digital data facilitate the integration of gravity and magnetic information with other geophysical and geological datasets, improving the

ability to create comprehensive 3D models and visualizations. This integration also ensures better accessibility and long-term storage, as digital formats are easier to share, archive, and maintain. The increased accuracy and resolution provided by digitization help to minimize errors from manual readings, enabling more reliable and higher-quality interpretations. Moreover, the transformation of analog data to digital allows for the application of automated workflows and machine learning models, which can quickly and accurately identify geophysical anomalies and patterns. In essence, the conversion of analog gravity and magnetic data into digital formats modernizes legacy datasets, making them valuable for current research and exploration (Hinze et al, 2013). This process ensures that historical data remain useful in conjunction with modern technologies to address contemporary geophysical challenges, driving advancements in resource exploration and geohazard assessment.

The aim of this study is to understand the crustal characteristics of the South Marmara region, a tectonically active region, using geophysical data. In this context, the (YDABCAG-198Y231G) grid data obtained from the digitization of the Aegean region analog data have been regionally differentiated. In this way, the advantages and disadvantages of the general models and the models we have developed will be discussed.

Regional Geology of Marmara Region

Marmara Region of Turkey is a tectonically active and geologically complex region which located at the meeting point of the Anatolian and Eurasian plates (Figure 1A). The North Anatolian Fault Zone (NAFZ), a significant strike-slip fault system that permits the Anatolian Plate to move westward in relation to the Eurasian Plate, is responsible for its formation (Yaltrak, 2002). Many

structural and lithological features, such as the Sakarya Zone, the Thrace-Kocaeli Peneplain, the Armutlu-Almacık Highlands (Figure 1B), and several other significant elements, are the product of this tectonic context (Siyako et al.1989). These characteristics are essential to the region's current seismic activity in addition to providing insight into its geological past.

The pre-Cenozoic metamorphic and magmatic rocks (Figure 1C) that make up the Armutlu-Almacık Highlands are elevated chunks of old crust (Yaltrak et al.1998; Sakıncı et al.1999; Duru et al..2012). These highlands, which are situated near the southern edges of the Marmara Sea, have been greatly impacted by the NAFZ's tectonic activity (Yaltrak et al. 2000; Yaltrak, 2002). The region's early tectonic activities, such as the collision and accretion of crustal fragments during the Mesozoic and Cenozoic eras, can be understood from its geological composition (Yaltrak et al. 2000; Yaltrak and Alpar, 2002).

The Sakarya Zone, located southeast of the Marmara Region, is a tectonostratigraphic region that contains Mesozoic to Cenozoic sedimentary and volcanic rocks. This zone is part of the Anatolian tectonic framework and represents the closing of the Neotethys Ocean and the subsequent Alpine orogeny (Okay and Tüysüz, 1999). The Sakarya Zone's structure and strata provide excellent evidence of the intricate interactions between tectonic plates that occurred during the region's geological development (Şengör and Yılmaz 1981; Le pichon et al.,2001).

The Thrace-Kocaeli Peneplain is a large, relatively flat terrain stretching from the Thrace Basin in the northwest to the Kocaeli Plateau in the east. This peneplain, underlain by sedimentary and basement rocks, is an old erosional surface that has been altered by tectonic uplift and faulting. It plays an important role in connecting the Thrace Basin's geological history to that of the Marmara. Other notable tectonic structures include the Strandja Massif, located to the north and composed of older metamorphic and intrusive rocks that connect the Marmara Region to the Balkan orogenic system (Şengör and Yılmaz 1981). The Uludağ Massif, located to the south, is a prominent geological structure. Its metamorphic and granitic rocks reflect the region's tectonic uplift and magmatic history (Kaymakçı,1991; Imbach,1992; Eisenlohr, 1995). The tectonic terrain beneath the Sea of Marmara is dominated by pull-apart basins, including Çınarcık, Tekirdağ, and Central Basins, as well as intervening structural highs (Yaltrak et al. 2000; Yaltrak and Alpar,2002). These basins are the direct result of extensional processes along the NAFZ, and they include thick sedimentary deposits.

The tectonic features of the Marmara Region offer a singular chance to investigate the interaction between active tectonics and old geological processes. Recognizing these characteristics is crucial for determining seismic threats in this geologically active zone as well as for reconstructing the region's geological past. Exploring the relationships between these tectonic

features and their consequences for regional geodynamics and earthquake risk management will require more thorough research backed by geological surveys and seismic data.

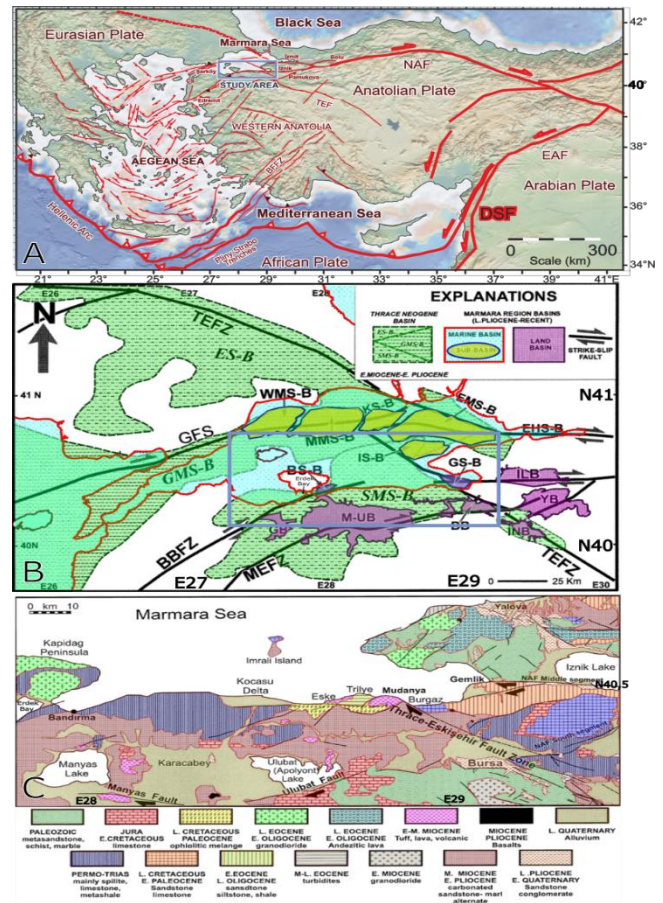


Fig. 1A. Location map of the study area and general tectonics of Turkey (Yaltrak et al., 2012; NAF: The North Anatolian Fault, TEF: Thrace-Eskişehir Fault, EAF: East Anatolian Fault, BFFZ: Burdur-Fethiye Fault Zone , DSF: Dead Sea Fault . 1.B) Main tectonic elements of Marmara Region (TEFZ: Thrace-Eskişehir Fault, GFZ: Ganos Fault, BBF: Bandırma-Behramkale Fault and MEFZ Manyas-Edremit Fault Zones; ES-B: Ergene, GMS-B: Gelibolu-Marmara; SMS-B: South Marmara; WMS-B: West Marmara, MMS-B: Middle Marmara, KS-B, Kumburgaz, EMS-B: East Marmara; BS-B: Bandırma, GS-B: Gemlik; EHS-B: Izmit Sub-basins, ILB: Iznik Lake, YB: Yenişehir; INB: Inegöl, BB: Bursa, M-UB: Manyas-Uluabat; GB: Gönen Basins C) Geology map of the study area. (E: Early, L: Late, M: Middle (Vardar et al., 2014).

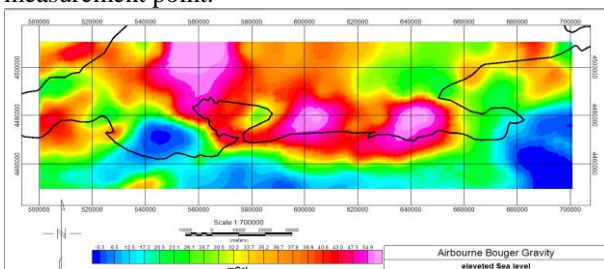
Materials and Methods
Airborne Gravity and Magnetic

In this study, the discrimination of gravity and magnetic data of the Marmara region has been regionally enhanced. The data were provided by the YDABCAG-198Y231G project. The majority of published research papers applied the Tilt-depth (Oruç, 2011) approach to a gravity or magnetic anomaly caused by a shallow source, indicating that the Tilt-depth method is accurate. Salem et al. (2013) proposed a way for determining the magnetic tilt-depth of a shallow source using gravity measurements. Cooper was a pioneer in applying a comparable tilt-depth

methodology to gravity data in 2011 and 2012, using vertical cylinder and sphere models. Salem et al. (2013) established the method's practical value by using full tensor gravity gradiometry (FTG) data to obtain more precise geological results. To determine the gravity and magnetic tilt-depth, the top depth can be estimated by subtracting the distance between the +45 and -45 degrees contours from the tilt angle, which is simple to apply; however, previous research has used different rulers. Cooper (2012,2014), for example, determined the depth to the source by identifying circular contours, as well as the radius and value of the contour; Salem et al. (2007,2013) estimated the location and depth of causative gravity sources using only the three vertical components of the FTG data (T_{zx} , T_{zy} , and T_{zz}) with a scale value related to the anomaly of the nature source. The average crustal thickness of the region was calculated and crustal modelling was performed. In addition, the isostatic anomaly of the region was calculated and its effect on the gravity data was removed.

Gravity Data

The gravity data used in this study consists of the values measured between 1975 and 1988 within the framework of the "Turkey's Regional Gravity" project of the General Directorate of Mineral Research and Exploration, Department of Geophysical Studies. In this project, measurements were taken at certain roper points, mainly reference point, located on 1:25000 topographic maps. The maximum distance between measurement points is 1 km and approximately 65000 data were collected in the study area. The latitude was corrected according to the international gravity formula (1967). The Bouguer density of 2.67 gr/cm3 was chosen for the calculation of the Bouguer gravity values. The terrain correction took into account the effect of the masses within the setcores with a radius of 167 km, the centre of which is the measurement point.



In the initial phase, we endeavored to calculate surface functions that would traverse each measurement point. In calculating the surface functions, we found it most effective to use the measurement point to be represented by the surface, along with the 30 measurement values closest to this point. We weighted the effects of these closest notes on the surface function based on their distance from the point for which the surface function was to be calculated. In addition, we ensured that the value of each surface function on the coordinates it belongs to matches the value measured at that point.

In the second stage, we sought to obtain the values at each grid point by using the surface functions of the 30 points that were in closest proximity to that grid point. During this process, we endeavored to apply a similar weighting based on the distances as in the first stage. In the event that a grid point is in alignment with a measurement point, the value recorded at that grid point is deemed to be the most appropriate. The aforementioned gridding method was applied to the measured gravity values and Bouguer gravity and magnetic anomaly values, with a sampling interval of 0.5 km being obtained. We hope that the gravity anomaly map of the region, created using this method, will be of interest and use to you. You will find it in Figures 2 and 3.

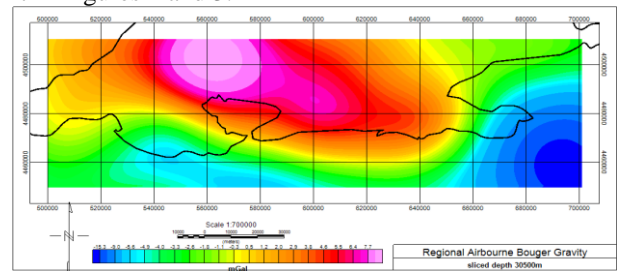


Fig. 1. Bouguer gravity map (elevated to sea level)

In this study, we had the privilege of using data from the 1:500,000 scale maps of Istanbul, Balıkesir and Bursa. Furthermore, data for the Sea of Marmara were kindly provided by C&K Petroleum (1978) in the form of their airborne gravity and magnetic maps of the region. A variety of methods were explored for sampling the randomly distributed data at regular intervals. Through this process, it became evident that the method which samples the data based on the distance between the measurement points may offer a promising approach. We believe that this method has proven to be more successful than others because it considers the physical dimensions of the data in question. The gridding process was conducted in two stages.

Fig. 2. Regional Bouguer gravity map of sliced depth approx. 30 km

Magnetic Data

The magnetic data which were obtained by an airborne proton magnetometer between 1978 and 1990 were used in the study. During this period, we had the opportunity to fly 446,700 km and survey an area of 813,639 km². Wherever possible, flight altitudes were kept at 2000 feet above the topography. The distance between profiles was adapted according to geological information, with a variation of 0.5–1 km.

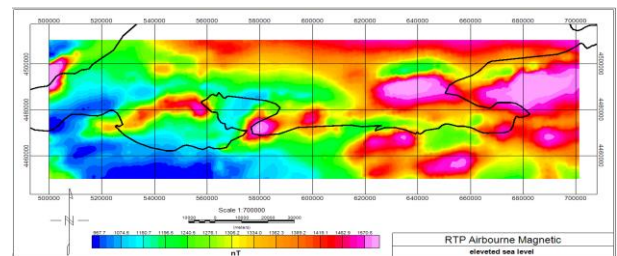


Fig. 3. Reduced to pole (RTP) Airborne Magnetic Data (elevated sea level)

It was our understanding that the flight lines were laid out in a way that was perpendicular to the geological features. In the study area, a fixed proton magnetometer was also positioned onshore, with the aim of measuring daily

variations simultaneously for later correction. Additionally, magnetic data were compared with Mayer et al. (2017) satellite data. The recordings were initially acquired in analogue format and subsequently converted to digital. During this process, we took into account the severity of the anomaly and took samples at 100-metre intervals in areas with fast variations, while in calm areas we increased the sampling interval to 0.5 km. In order to account for daily variations, the measured values were reduced to October 1982. It should be noted that the International Geomagnetic Reference Field (IGRF) variations were not taken into account in this data set. Therefore, IGRF correction was also made on the gridded values (Peddie 1982).

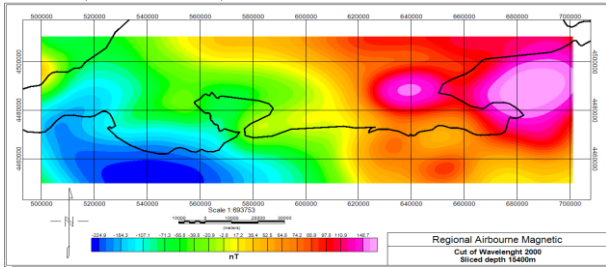


Fig. 4. Regional RTP Airborne Magnetic Data (sliced depth 15400 m, Cut of wavelength 900)

The all data (magnetic and gravity) were then adjusted to sea level using the downward extension method, taking into account the topography. We proceeded to remove virtual interferences in the reduced data using a Hanning filter. The data obtained as a result were then subjected to a first-order Butterworth filter, with the cut-off wavelengths of the low-pass filter expressed in units of location at the half-amplitude point, which was found to be 1500. We then proceeded to take the horizontal (x,y), vertical derivatives and horizontal gradient (THD) of our data (Oruc,2011; Hinze,2013). We then used these gradients to determine the tilt angle. This was followed by the estimation of depths over the grid. The grids whose tilt angles were determined were first taken into absolute value, and then the measurable depths were obtained on the graph with the help of a mathematical function (Salem, 2007; Oruc, 2011). In this function, the absolute value results were passed to the ones less than $\pi/4$, while the other parts were left blank(null).

Results

Gravity Data

The gravity anomalies changes from -5,3 to 54,9 in the study area. The highest anomalies seen in the marine and coastal area. However the direction of the highest anomalies changes to North at the western Kapıdağ peninsula. In Erdek bay the lowest values are observed (Figure 2). At the Southern part and the easternmost of the study area the low anomalies can be observed too. The sliced depth anomaly map for 30 km which shows the anomaly values of the 30 km depth base rocks anomalies increase to the North West (to the marine area, Figure 3). The vertical and horizontal derivatives of bouguer anomalies are given in Figure 6. The derivative of x-y (Figure 6a) showed that the source of the maximum anomalies is still in the same location that seen in Fig 2

(bouguer anomaly map). Total horizontal derivative map that shown in Fig 6a indicated that the boundaries of the structure which provided the main anomalies.

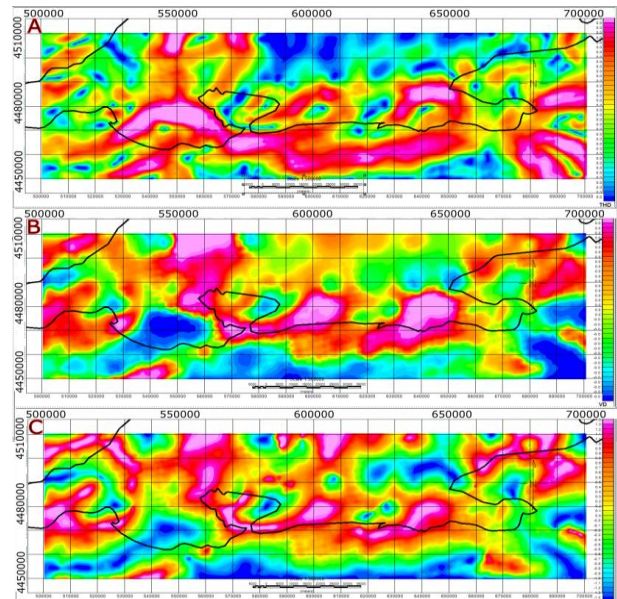


Fig. 5. The vertical and horizontal derivatives of bouguer anomalies; (a) THD-Total Horizontal Derivative (dx&dy), (b) VD-1st Vertical derivative, (c) Tilt derivative (tilt).

Magnetic Data

The magnetic values are reached the highest values at the Armutlu Peninsula and the offshore of Peninsula (Figure 4). In Bandırma bay magnetic anomlies are relatively high.

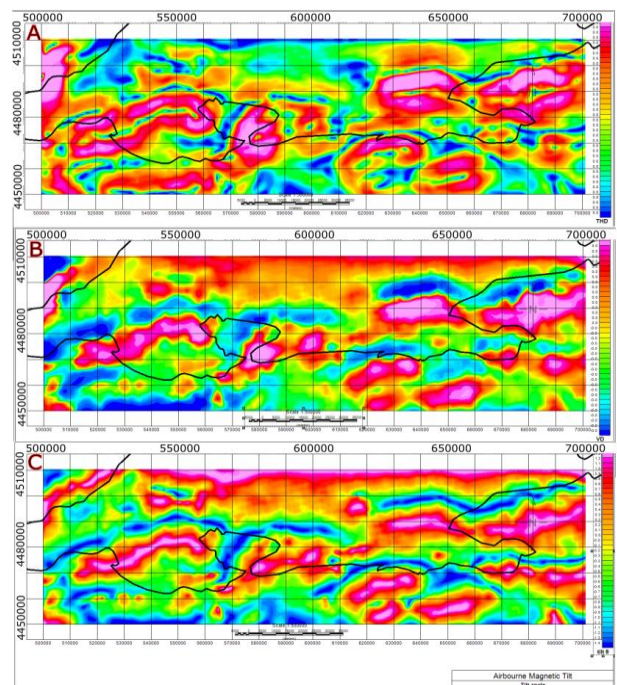


Fig. 6. The derivatives of magnetic anomalies; (a) THD-Total Horizontal Derivative (dx&dy), (b) VD-1st Vertical derivative, (c) Tilt derivative (tilt).

The other high values are observed at the western part of Kapıdağ Peninsula and The South West onshore part of study area (Figure 4). The Eastern part of the study area

the lowest values spread to wider area. According to the sliced depth anomaly map for 15 km the magnetic anomalies general trend is decreasing values from east to West (Figure 5). The vertical and horizontal derivatives of magnetic anomalies are given in Figure 7. The derivative of x-y (Figure 7a) showed that the source of the maximum anomalies is still in the same location that seen in Fig 4 (magnetic anomaly map). Total horizontal derivative map that shown in Fig 7a indicated that the possible boundaries of the magnetic featured structure.

Radially Averaged Power Spectrum (RAPS) with depth-slice

The Fast Fourier Transform (FFT) is a technique employed for the purpose of transforming a grid into and from the wavenumber domain. The data set that is equivalent to the original set in the wavenumber domain is referred to as a "transform". The transform is constituted of wavenumbers, comprising both real and imaginary components. The grid samples a space domain function at even distance increments, whereas the transform samples the Fourier domain function at even increments between 0 and the Nyquist wavenumber. The potential field function in the space domain has a unique wavenumber domain function, and vice versa. The power spectrum is a two-dimensional function of power relative to wavenumber and direction. The RASP is calculated by averaging power for all directions for the same wavenumber. The Fourier transform of a prismatic body's potential field has a broad spectrum, with its peak location determined by the prism's density or magnetisation.

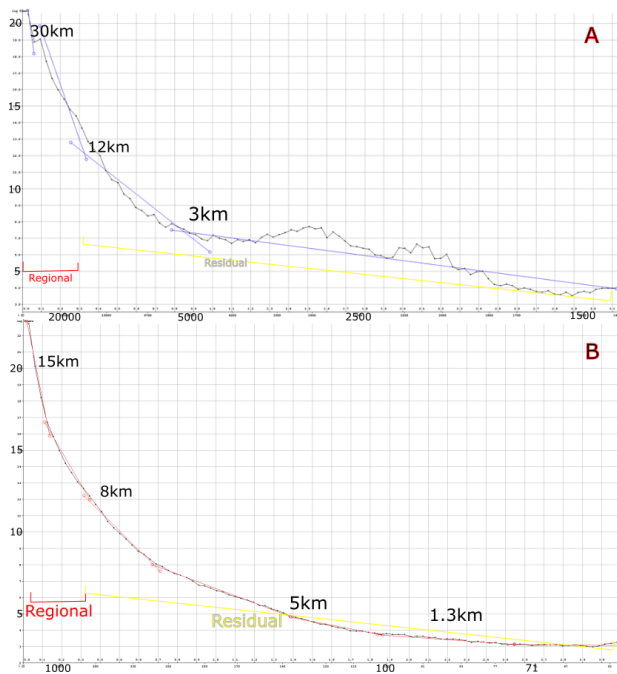


Fig. 7. Radially averaged power spectrum of Bouguer gravity(A) and magnetic(B) with sliced depths.

The objective of processing the Bouguer gravity and magnetic data is to determine lineament patterns for different physical depths, thereby gaining a three-dimensional appreciation of the structures. This objective can be achieved by performing a Fast Fourier Transform (FFT) on depth slices of the top basement from the data set (deep component), as well as top to mid and shallow wavelength Bouguer gravity and magnetic sources maps. Depth slicing is a technique employed for the purpose of differentiating between regional and residual components of a potential field data set (Spector and Grant, 1970). The process entails the examination of the log power spectrum and the identification of linear segments, the simplicity of which is contingent upon the data and the contributing source bodies. In this instance, the initial, deeper line segment was selected with greater confidence than the two subsequent ones (Fig. 8). When contemplating a grid that encompasses a multitude of sources, the log spectrum of this data can be interpreted to ascertain the statistical depth to the summits of the sources. The power spectra (Fig. 8) demonstrate that the deepest structures are observed at 30 km in the gravity data set and at 15 km in the magnetic data set. Furthermore, regional and residual anomalies were distinguished in accordance with the indications provided by these graphs. In the Bouguer gravity data set, a single-pass Butterworth filter and a low-pass filter with a cut-off of 1500 were applied; in the magnetic data set, a low-pass filter with a cut-off of 900 was applied, and regional anomalies were reached. Furthermore, the depth-slice method enabled the determination of the depths of the structures causing gravity anomalies, which were found to be approximately 30 km, 12 km, and 3 km. Similarly, the depths of the anomalies causing magnetic anomalies were determined to be approximately 15 km, 8 km, 5 km, and 1.3 km. Additionally, separate tilt depth grids of the structures at these depths were created and examined (figure 9-10).

Bouguer Gravity tilt-depth

The figures below illustrate the depth-sliced layers of the Bouguer gravity data and the tilt depth grid of the entire data set. The depths of the near-surface structures affecting the anomaly, situated at approximately 3 km below the surface (Figure 9a), were found to vary between 1 and 1.5 km on average. The tilt-depth solution of the structures affecting the anomaly at an average depth of 5300 m (Figure 9b) revealed the presence of a structure associated with the uplift between the Gemlik subbasin and the Armutlu Peninsula, with a depth of approximately 9 km in the south of the Armutlu Peninsula.

The structure, which is believed to be responsible for the fundamental uplift of Imralı Island, was observed to have a length of approximately 4 km in the north and 3.5 km in the south. The structure responsible for the uplift between the Armutlu Peninsula and Imralı Island was determined to be approximately 3.5 km in depth.

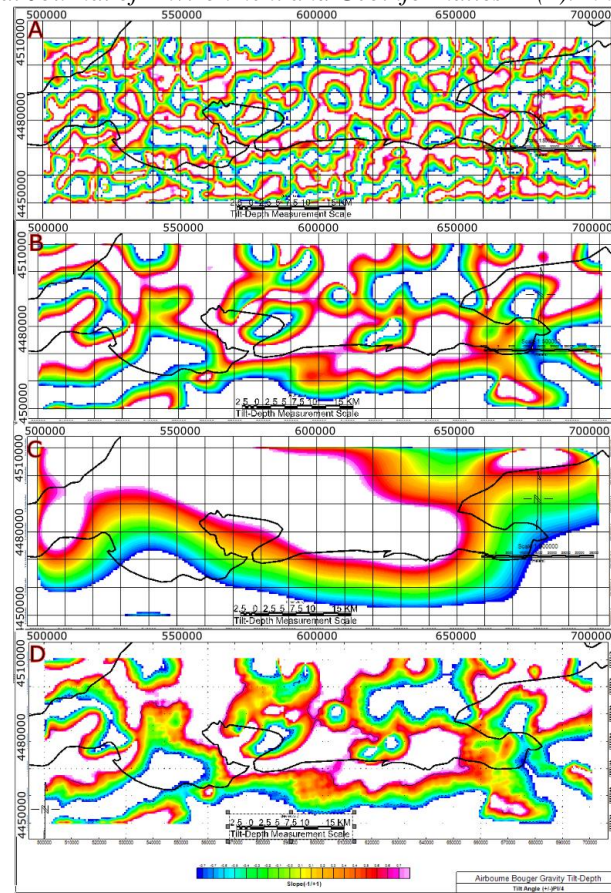


Fig. 8. The tilt depths of sliced gravitational structures for (a) 3km, (b) 12km, (c) 30 km and total gravity.

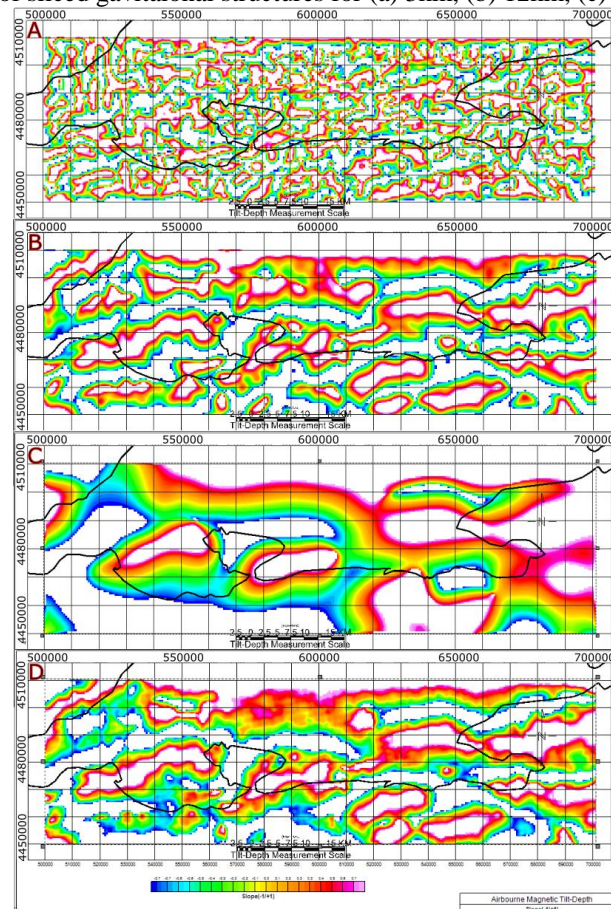


Fig. 9. The tilt depths of sliced magnetic structures for (a) 1.3km, (b) 8km, (c) 15 km and total magnetic.

It was determined that the mass responsible for the anomaly observed in the northern region of Kapıdağ Peninsula, situated around Marmara Island, is attributable to the 2 km wide structures identified within the 5 km depth grid. In general, the depths of the structures observed in this grid were found to be, on average, 2.5 km. The mass boundary responsible for the primary anomaly was unambiguously delineated with a grid of approximately 30 km depth (Figure 9c). In this grid, it was determined that the structure, which was measured at a depth of approximately 9 km, originated from the north of Armutlu Peninsula and continued in a south-easterly direction, ultimately reaching the west of the coastal bank. Figure 9d presents the results of a Bouger anomaly analysis conducted using the tilt depth method. The findings indicate that the structures responsible for the observed anomalies are similar to those identified in figure 9b. Consequently, it can be inferred that these structures extend from the surface to an average depth of 7-15 km.

Airborne Magnetic tilt-depth

Figure 10 illustrates the depth-sliced layers of air magnetic data and the tilt depth grid of the entire area. It was established that the depths of the structures in the vicinity of the surface that are responsible for the anomaly are situated at an approximate depth of 0.5 km below the surface (Figure 9a), with a mean range of 0.3-1 km. The tilt-depth solution, calculated at an average depth of 5100 m for the structures affecting the anomaly (Figure 10b), revealed the presence of a structure approximately 1.5 km deep in the south of the Armutlu Peninsula. This structure was hypothesised to be associated with the uplift between Gemlik subbasin and Armutlu Peninsula. The structure hypothesised to be responsible for the foundation uplift of Imrayi Island was found to have a length of approximately 3.9 km in the north and 1.5 km in the west. The structure responsible for the observed uplift between the Armutlu Peninsula and Imrali Island was determined to have an average depth of approximately 2 km. It was thus determined that the mass responsible for the anomaly observed in the vicinity of Marmara Island, originating from the 2.9 km wide structures detected at a depth of 5 km, was the source of the anomaly seen around Marmara Island from the north of Kapıdağ Peninsula. Furthermore, the boundaries of the Bandırma Sub-basin (BS-B) were found to lie between 1.9 and 2.7 km within this gyre, while the structure boundary of the Gemlik Sub-basin (GS-B) was measured at 1.7 km. In general, the depths of the observed structures in this gyre were found to be approximately 2.2 km on average. The mass boundary responsible for the fundamental anomaly was definitively identified with the approximately 15 km deep grid (Figure 10c). The boundaries of the Bandırma Sub-basin (BS-B) were found to be 3.4 km wide, while the Gemlik Sub-basin (GS-B) exhibited structure boundaries of approximately 2.7 km in width. It was established that the structure, which was measured at a depth of approximately 6.7 km in this grid, continued in a westerly direction along the coast from the south of Armutlu Peninsula to the study area. Figure 10d presents the entirety of the airborne magnetic anomaly, reduced to sea

level, and examined with the tilt depth method. It was determined that the structures causing the anomalies were similar to those observed in Figure 10b, and thus the structures causing the anomalies extended to an average depth of 2.5-4.9 km from the surface. According to the study conducted in İznik Lake in the east of our study area (Aktaş et al, 2021), similar structures were examined in more detail and similar results were obtained.

Discussion

The most prominent feature of the gravity values reduced to sea level is that these values are high in the marine area. Relatedly, the elevation in the eastern part is around Imrali Island and the other highest anomaly values are close to the east of Kapıdağ Island and in the regions north of Kapıdağ Island and Marmara Island. These values observed in areas with islands and high topography indicate that a tectonic effect increased the values in this area. In addition, the geological formations in areas with high gravity values are granodiorite and Permian limestone. In addition, riverine and lacustrine influences are effective in all areas with low values. These rivers accumulate the material they carry in these areas and decrease the gravity values. Late Quaternary alluviations are active in these areas.

The most readily apparent consequence of the gravity anomaly is the observed increase in gravity values from east to west. Given that this increase is observed across the entire map, it can be posited that it is influenced by the crustal mantle boundary. Similarly, seismic studies conducted by Kutel et al. (1996) demonstrate that the velocity of seismic waves is higher in this region than in the southern parts.

The elevated sea level magnetic map (Figure 10d) shows that high and low values generally follow a uniform geomorphology. In this context, it is consistent with the NAF middle strand geometry given in the article of Vardar et al. 2014;2021, a tectonic study conducted in the region. The study suggests a segmented mechanism starting from Gemlik Bay and going to Bandırma Bay. Previously, a higher resolution marine magnetic study was conducted in Gemlik Bay and this study revealed the tectonic details of Gemlik Bay (Aktaş et al.2023). Although our study detected similar structures and depths in the same region, Aktaş et al. (2023) applied the edge detection methods for structures. The fault geometry is consistent with low and high anomaly boundaries. In addition, in the same study, a pressure ridge is suggested for Bandırma Bay. The gradient of magnetic values here are consistent with those structural elements. A fault system passing south of Marmara Island is also given in Vardar et 2016. In general, magnetic distributions in study are related with main tectonic factors. The increase in magnetic anomaly values over the depressions in the Marmara Sea indicates the potential for magma intrusions into these depressions, given the extremely low magnetisation of the sediments. Furthermore, the fact that these anomalies are observed only as a single inclusion

strengthens the possibility that the strata here are rather parallel to the Earth's surface.

In the studies conducted by Ateş, A. et al. (2012), Ekinci, and Yiğitbaş (2015), Bilim, F. et al. (2021), and Özsöz and Toker (2022), the crustal thickness for the study area was determined to be between 25 km and 36 km. In the present study, the maximum crustal thickness was calculated to be 30.5 km. In this context, it is evident that studies focusing on the region yield more significant results. In general terms, given that the region is a transition zone, the crustal thickness for the Black Sea was calculated to approximately 33 km (Ekinci and Yiğitbaş, 2015) and the Aegean 29 km (Özsöz and Toker). As calculated in our study, the reason why the crustal thickness is approximately 30 km in the south of the Marmara Sea is that it is formed as a result of the opening between these two seas. As a consequence of this stretching, the NAF is divided into three branches in western Anatolia.

Conclusion

We have used gravity and magnetic data to image and characterize the structure and composition of the Earth's upper crust between the Gemlik Bay and Kapidag Peninsula, South Marmara, using the Tilt-Depth and Depth slicing from Power Spectrum method to determine the depths of structures. Similarly, in another study conducted in İzmit Bay, the compatibility of magnetic data was revealed by examining the structures together with 2D seismic data (Aktaş and Demirel, 2024). For this reason, we would like to emphasize that it is important to evaluate the previously obtained seismic data in the study area (Vardar et al. 2014, 2016) together with our gravity and magnetic data set in order to obtain more detailed information. The application of the Tilt-Depth method allows us to better define the subsurface geology of Southern Marmara Region. Our results are in general agreement with interpretations based on geological mapping and structural analyses, and we are able to trace regional stratigraphy and tectonic boundaries such as the central segment of the NAF based on potential field data.

References

Adatepe, F., Demirel, S., Alpar, B., (2002). Tectonic setting of the southern Marmara Sea region: based on seismic reflection data and gravity modelling. *Marine Geology*, vol.190, 383-395.

Aktaş, G., Demirel, S., (2024). Application of edge detection methods to İzmit Gulf magnetic data. *Gümüşhane Üniversitesi Fen Bilimleri Dergisi*, vol.14, no.1, 300-312.

Aktas, G., Hisarlı, Z. M., Demirel, A. S., (2021). High-resolution total field magnetic anomaly maps of Lake Izmit (NW Turkey): assessment of faults which play important roles in tectonics of the lake. *Marine Geophysical Research*, vol.42, no.3.

Aktaş, G., Hisarlı, Z. M., Demirel, A. S., (2023). Interpretation of the tectonic structure of Gemlik Bay using magnetic data. *Tectonophysics*, vol.863.

Ateş, A., Bilim, F., Buyuksarac, A. et al (2012).. Crustal Structure of Turkey from Aeromagnetic, Gravity and Deep Seismic Reflection Data. *Surv Geophys* 33, 869–885 <https://doi.org/10.1007/s10712-012-9195-x>

Bilim, F., Aydemir, A., Ateş, A., Dolmaz, M. N., Koşaroğlu, S., Erbek, E., (2021). Crustal thickness in the Black Sea and surrounding region, estimated from the gravity data. *Marine And Petroleum Geology*, vol.123.

Blakely, R. J. (1995). *Potential Theory in Gravity and Magnetic Applications*. Cambridge University Press.

Cooper, G. R. J. (2012). A gradient-ratio method for the semiautomatic interpretation of gravity map data sets. *Geophysical Prospecting*, 60, 995-1000.

Cooper, G. R. J. (2014). The automatic determination of the location, depth, and dip of contacts from aeromagnetic data. *Geophysics*, 79(3), J35-J41.

Duru, M., Dönmez, M., Ilgar, A., Pehlivan, Ş., Akçay, A. E. (2012). *Geological map of the Biga Peninsula, scale: 1/250000*. Ankara: MTA (General Directorate of Mineral Research and Exploration of Turkey) Publications.

Eisenlohr, T., (1995). *Die Thermalwaesser der Armutlu-Halbinsel (NW-Turkei) und deren Beziehung zu Geologie und aktiver Tektonik (English abstract)*. ETH Zurich, 165 pp.

Ekinci, Y. L., Yiğitbaş, E. (2015). Interpretation of gravity anomalies to delineate some structural features of Biga and Gelibolu peninsulas, and their surroundings (north-west Turkey). *Geodinamica Acta*, 27(4), 300-319. <https://doi.org/10.1080/09853111.2015.1046354>

Ekşi, H., (1992). *Trilye (Zeytinbağları) güneydogusunun jeolojisi*. M.S. Thesis. Istanbul Technical University, 52 pp.

Hinze, W. J., Von Frese, R. R. B., Saad, A. H. (2013). *Gravity and Magnetic Exploration: Principles, Practices, and Applications*. Cambridge University Press.

Imbach, T., (1992). *Thermalwaesser von Bursa. Geologische und hydrogeologische Untersuchungen am Berg Uludağ (NW Turkei)* Diss Nr. 9988. ETH Zurich, 178 pp.

Kaymakçı, N., (1991). *Neotectonic evolution of the Inegöl (Bursa) basin*, M.Sc. Thesis. Middle East Technical University, 73 pp.

Le Pichon, X., Şengör, A. M. C., Demirbağ, E. (2001). The active tectonics of the North Anatolian Fault Zone in the Marmara Sea region. *Geophysical Journal International*, 144(3), 511-542.

Meyer B, Saltus R, Chulliat A (2017). *EMAG2: Earth Magnetic Anomaly Grid (2-arc-minute resolution) Version 3*. National Centers for Environmental Information. NOAA. Model. DOI: <https://doi.org/10.7289/V5H70CVX>

Milligan, P. R., Gunn, P. J., (1997), Enhancement and presentation of airborne geophysical data. *AGSO Journal of Australian Geology Geophysics*, 17(2), 63-75

Nabighian, M. N., Grauch, V. J. S., Hansen, R. O., LaFehr, T. R., Li, Y., Peirce, J. W., Phillips, J. D., Ruder, M. E. (2005). The historical development of the magnetic method in exploration. *Geophysics*,

- 70(6), 33ND-61ND.
<https://doi.org/10.1190/1.2133784>
- Okay, A. I., Tüysüz, O. (1999). *Tethyan sutures of northern Turkey*. Geological Society, London, Special Publications, 156(1), 475–515.
- Oruç, B. (2011) Edge Detection and Depth Estimation Using a Tilt Angle Map from Gravity Gradient Data of the Kozaklı-Central Anatolia Region, Turkey. *Pure Appl. Geophys.* 168, 1769-1780.
<https://doi.org/10.1007/s00024-010-0211-0>
- Özsöz, İ., Toker, C. E. (2022). Interpretation of satellite gravity anomalies with pseudo-depth slicing method filter in Türkiye. *Bulletin of the Mineral Research and Exploration*, 168(168), 111-130.
<https://doi.org/10.19111/bulletinofmre.974936>
- Peddie, N. (1982). International Geomagnetic Reference Field (IGRF). *J. Geomag. Geoelectr.*, 34, 308-326.
- Sakınç, M., Yaltrak, C., Oktay, F.Y., (1999). Palaeogeographical evolution of the Thrace Neogene Basin and the Tethian- Paratethian relations at northwest Turkey (Thrace). *Palaeogeogr. Palaeoclimatol. Palaeoecol.* 153, 17-40.
- Salem, A., William, S., Fairhead, J., Smith, R. (2007). Tilt-depth method: A simple depth estimation method using first-order magnetic derivative. *The Leading Edge*, 26(12), 1502-1505.
- Salem, A., Masterton, S., Campbell, S., Fairhead, J. D., Dickinson, J., Murphy, C. (2013). Interpretation of tensor gravity data using an adaptive tilt angle method. *Geophysical Prospecting*, 61, 1065-1076.
- Şengör, A. M. C., Yılmaz, Y. (1981). Tethyan evolution of Turkey: A plate tectonic approach. *Tectonophysics*, 75(3-4), 181-241.
- Siyako, M., Bürkan, K.A., Okay, A.I., (1989). Biga ve Gelibolu yarımadalarının Tersiyer jeolojisi ve hidrokarbon olanakları. *Bull. Turk. Assoc. Pet. Geol.* 1, 183-199.
- Siyako, M., Tanış, T., Şaroğlu, F., (2000). Marmara Denizi aktif fay geometrisi. *TÜBİTAK Bilim Tek. Derg.* 388, 66-71.
- Spector, A. and Grant, F. S. (1970), "Statistical models for interpreting ship-borne magnetic and gravity data", *Geophysics*, 45, 293-302.
- Vardar, D., Öztürk, K., Yaltrak, C., Alpar, B. and Tur, H. (2014). Late Pleistocene–Holocene evolution of the southern Marmara shelf and sub-basins: middle strand of the North Anatolian fault, southern Marmara Sea, Turkey, *Mar. Geophys. Res.*, 35, 69-85.
- Vardar, D., Alpar, B., (2016). High-Resolution Seismic Characterization of Shallow Gas Accumulations in the Southern Shelf of Marmara Sea, Turkey. *Acta Geophysica*, vol.64, no.3, 589-609.
- Vardar, D., Alp, H., Demirel, S., Aykurt Vardar, H., Alpar, B., (2021). Offshore/onshore correlation of the North-Anatolian fault deformations in the Western Sea of Marmara. *Natural Hazards*, vol.107, no.2, 1905-1923.
- Yaltrak, C., Alpar, B., Yüce, H., (1998). Tectonic Elements Controlling the Evolution of the Gulf of Saros (Northeastern Aegean Sea). *Tectonophysics* 300, 227-248.
- Yaltrak, C., Alpar, B., Sakınç, M., Yüce, H., (2000). Origin of the Strait of Canakkale (Dardanelles): Regional Tectonics and the Mediterranean Marmara incursion, *Marine Geology*. 164, 139-156, with erratum 167, 189-190.
- Yaltrak, C. (2002). Tectonic evolution of the Marmara Sea and its surroundings. *Marine Geology*.
- Yaltrak, C., Alpar, B., (2002). Evolution of the middle strand of North Anatolian Fault and shallow seismic investigation of the Southeastern Marmara Sea (Gemlik Bay). *Marine Geology*, this volume.